

# Pixel-wise Energy-biased Abstention Learning for Anomaly Segmentation on Complex Urban Driving Scenes

Yu Tian\*   Yuyuan Liu\*   Guansong Pang  
Fengbei Liu   Yuanhong Chen   Gustavo Carneiro  
Australian Institute for Machine Learning, University of Adelaide

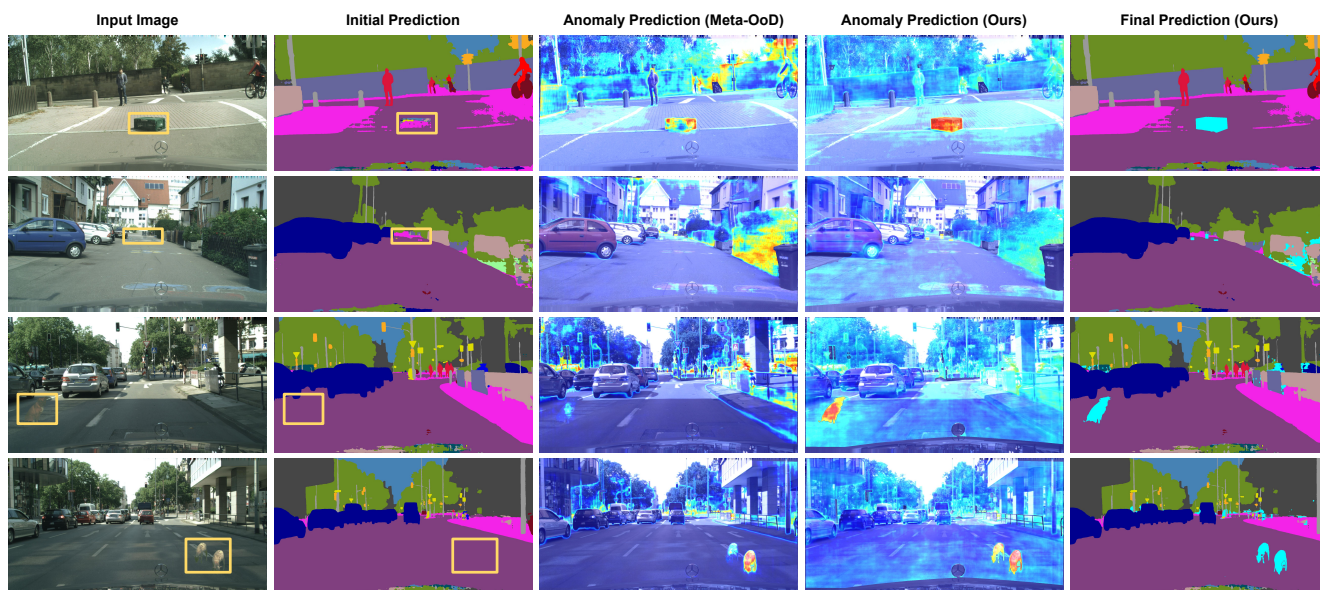


Figure 1. **Anomaly segmentation overview.** From the **input image** (anomaly highlighted with a yellow box), the **initial prediction** shows the original segmentation results with anomalies classified as a one of the pre-defined inlier classes. **Anomaly predictions** by the previous SOTA **Meta-OoD** [5] and **our** method show an anomaly map with high scores (in yellow and red) for anomalous pixels, where our approach shows less false positive and false negative detections. Consequently, our method can detect small and distant anomalies (row 2) and blurry/unclear anomalies (rows 1, 3, 4) more accurately than Meta-OoD [5]. In our **final prediction**, anomalous pixels are coloured as cyan. **Some anomalies are small and blurred (e.g., row 2), so please zoom in the PDF for better visualisation.**

## Abstract

*State-of-the-art (SOTA) anomaly segmentation approaches on complex urban driving scenes explore pixel-wise classification uncertainty learned from outlier exposure, or external reconstruction models. However, previous uncertainty approaches that directly associate high uncertainty to anomaly may sometimes lead to incorrect anomaly predictions, and external reconstruction models tend to be too inefficient for real-time self-driving embedded systems. In this paper, we propose a new anomaly segmentation method, named pixel-wise energy-biased abstention learning (PEBAL), that explores pixel-wise abstention learning (AL) with a model that learns an adaptive pixel-*

*level anomaly class, and an energy-based model (EBM) that learns inlier pixel distribution. More specifically, PEBAL is based on a non-trivial joint training of EBM and AL, where EBM is trained to output high-energy for anomaly pixels (from outlier exposure) and AL is trained such that these high-energy pixels receive adaptive low penalty for being included to the anomaly class. We extensively evaluate PEBAL against the SOTA and show that it achieves the best performance across four benchmarks. Code is available at <https://github.com/tianyu0207/PEBAL>.*

## 1. Introduction

Recent advances in semantic segmentation have shown tremendous improvements on complex urban driving

\*First two authors contributed equally to this work.

scenes [22]. Despite the accurate predictions on the inlier classes, the model fails to properly recognise anomalous objects that deviate from the training inlier distribution (col. 2 of Fig. 1). Addressing such failure cases is crucial to road safety for autonomous driving vehicles. For example, anomalies can be represented by unexpected objects in the middle of the road, such as a large rock or an unexpected animal that can be incorrectly predicted as a part of the road class, leading to potentially fatal traffic collisions.

Current methods [2, 4, 5, 10, 19, 29, 33, 38] to detect and segment anomalous objects in complex urban driving scenes tend to depend on classification uncertainty or image reconstruction. The association of high classification uncertainty with anomaly is intuitive, but it has a few caveats. For instance, classification uncertainty happens when samples are close to classification decision boundaries, but there is no guarantee that all anomalies will be close to classification boundaries. Furthermore, samples close to classification boundaries may not be anomalies at all, but just hard inlier samples. Hence, these uncertainty based methods may detect a large number of false positive and false negative anomalies. For example, Fig. 1 shows that the previous SOTA Meta-OoD [5] misses important anomalous pixels (all rows), while misclassifying anomalies (e.g., vegetation in rows 1, 2, 3), even with the use of the outlier exposure (OE) strategy [18]. In fact, the OE strategy maximises the uncertainty for proxy anomalies, which can cause the model to be more uncertain for all inlier classes and detect false positive anomalies (e.g., Meta-OoD mis-classifies trees or bush with high anomaly scores – Fig. 1 col 4).

Reconstruction methods [10, 38] add an extra network to reconstruct the input images from the estimated segmentation, where differences are assumed to be anomalous. Not only does this approach depend on accurate segmentation results for precise reconstruction, but they also require an extra reconstruction network that is hard to train and inefficient to run in real-time self-driving embedded systems. Furthermore, previous approaches [2, 5, 10, 19, 29, 36] ignore a couple of important constraints for anomaly segmentation, namely smoothness (e.g., Meta-OoD fails to classify neighbouring anomaly pixels in Fig. 1, rows 1, 4) and sparsity (e.g., Meta-OoD incorrectly detects a large number of anomalous pixels—see yellow and red regions in Fig. 1, rows 1, 2, 3). Another common issue shared by previous methods [2, 5, 29] is that they usually rely on the re-training of the entire network for OE, which is inefficient and can also bias the classification towards outliers.

In this paper, we propose a new anomaly segmentation method, the pixel-wise energy-biased abstention learning (PEBAL), that directly learns a pixel-level anomaly class, in addition to the pre-defined inlier classes, to reject/abstain anomalous pixels that are dissimilar to any of the inlier classes. It is achieved by a joint optimisation of a novel

pixel-wise anomaly abstention learning (PAL) and an energy based model (EBM) [13, 23, 30]. Particularly, abstention learning (AL) [31] was originally developed to learn an image-level anomaly class, which is significantly challenged by the pixel-wise anomaly segmentation task that requires pixel-level anomaly class learning. This is because the original AL model treats all pixel inputs equally with a single pre-defined fixed penalty factor to regularise the classification of anomalous pixels, while adaptive penalties are typically required for different pixels in a complex driving scene, e.g., pixels in small (distant) objects vs. large (near) objects, or centred pixels vs fringe pixels of objects. PEBAL is designed to address this issue by learning adaptive pixel-wise energy-based penalties, which automatically decreases the penalty for pixels that are likely to be anomalies. Hence, our model does not explore previously proposed uncertainty measures (e.g., entropy or softmax criteria) or image reconstruction, and instead, for the first time, explicitly learns a new pixel-wise anomaly class. The learned penalty factors are jointly optimised with EBM, resulting in a mutually beneficial optimisation of anomaly and inlier segmentation. Additionally, we impose smoothness and sparsity constraints to the learning of the anomaly segmentation by PEBAL, incorporating local and global dependencies into the pixel-wise penalty estimation and anomaly score learning. Finally, the training of PEBAL is efficient given that we only need to fine-tune the last block of the segmentation model to achieve accurate inference. To summarise, our contributions are the following:

- We propose the pixel-wise energy-biased abstention learning (PEBAL) that jointly optimises a novel pixel-wise anomaly abstention learning (PAL) and energy-based models (EBM) to learn adaptive pixel-level anomalies. PEBAL mutually reinforces PAL and EBM in detecting anomalies, enabling accurate segmentation of anomalous pixels without compromising the segmentation of inlier pixels (cols. 4,5 of Fig. 1).
- We introduce a new pixel-wise energy-biased penalty estimation, which can learn adaptive energy-based penalties to highly varying pixels in a complex driving scene, allowing a robust detection of small/distant and blurry anomalous objects (Fig. 1 row 2).
- We further refine our PEBAL training, using a novel smoothness and sparsity regularisation on anomaly scores to consider the local and global dependencies of the pixels, enabling the reduction of false positive/negative anomaly predictions.

We validate our approach on Fishyscapes leaderboard [4], and achieve SOTA classification accuracy on all relevant benchmarks. We also achieve the best classification results on LostandFound [35] and Road Anomaly [29]

test sets, significantly surpassing other competing methods. We also show that our approach produces competitive pixel-wise calibration results on Cityscapes [8].

## 2. Related work

**Uncertainty-based Anomaly Segmentation.** Early uncertainty-based methods [17, 24, 27] focused on the estimation of image-level anomalies, but they tended to misclassify object boundaries as anomalies [19]. Jung et al. [19] mitigate this issue by iteratively replacing false anomalous boundary pixels with neighbouring non-boundary pixels that have low anomaly score. In [20, 21, 33], the boundary issue was tackled with a pixel-wise uncertainty estimated with MC dropout, but they showed a low pixel-wise anomaly detection accuracy [29]. Without fine-tuning using a proxy outlier dataset, uncertainty estimation may not be accurate enough to detect anomalies and can predict high uncertainty for challenging inliers or low uncertainty for outliers due to overconfident misclassification.

**Reconstruction-based Anomaly Segmentation.** Anomalies can also be segmented from the errors between the input image and its reconstruction obtained from its predicted segmentation map [1, 7, 9, 10, 15, 29, 38]. Those approaches are challenged by the dependence on an accurate segmentation prediction, by the complexity of reconstruction models that usually require long training and inference processes, and also by the low quality of the reconstructed images.

**Anomaly Segmentation via Outlier Exposure.** Hendrycks et al. [18] propose the outlier exposure (OE) strategy that uses an auxiliary dataset of outliers that do not overlap with the real outliers/anomalies to improve the anomaly detection performance. This OE strategy uses outliers from ImageNet [2, 3, 37], void class of Cityscape [10] or COCO [5], where the expectation is that the model can generalise to unseen outliers. Maximising uncertainty for outliers using the OE strategy can lead to a deterioration of the segmentation of inliers [3, 37]. Another major drawback of OE methods is that they are trained using outlier images or objects without considering the fact that outliers are rare events that appear around inliers. Hence, the training contains a disproportionately high amount of outliers [5] that can bias the segmentation toward the anomaly class. We address this issue by respecting the anomaly detection assumption, where anomalous objects are rare, contribute to a small proportion of the training set, and appear around inliers.

**Abstention Learning.** The abstention learning mechanism [11] adds a "reserve" class that is predicted when the classification predictions for all inlier classes are not high enough. Although this method was able to detect an anomalous image, we argue that it can be adapted to pixel-level classification with a modification on the training process to replace the pre-defined penalty factor for the whole training

set by an adaptive pixel-wise penalty. It is worth noting that differently from uncertainty-based methods [4, 5, 16, 19] that assume anomaly even when the model is uncertain but confident, abstention learning requires all classes to have low confidence to predict the anomaly class.

**Energy-based Models.** EBM is trained such that inlier training samples have low energy, whereas non-training outlier samples (i.e., anomalies) are expected to have high energy [23]. This energy value can then be used to compute the probability of a sample to belong to the inlier distribution. Recently, EBMs are being implemented with deep learning models [13, 30, 34], and to learn them, it is necessary to compute the partition function, which is generally estimated with Markov Chain Monte Carlo (MCMC) [13], but this estimation cannot generate accurate high-resolution images. Hence, we follow the simpler idea of estimating the energy score with the *logsumexp* operator [13, 30], where we minimise the energy of inliers and use an OE strategy [18] to maximise the energy of outliers. Hence, we do not need to compute the partition function.

## 3. Method

We present our PEBAL in this section (see Fig. 2), where we first describe the dataset, then introduce abstention learning and EBM. Next, we present the loss function to train the model, followed by the training and inference procedures, where we describe our AnomalyMix, which is a new way of forming the dataset of outlier samples.

### 3.1. Training Set

We assume to have a set of inlier training images and annotations  $\mathcal{D}^{in} = \{(\mathbf{x}_i, \mathbf{y}_i^{in})\}_{i=1}^{|\mathcal{D}^{in}|}$ , where  $\mathbf{x} \in \mathcal{X} \subset \mathbb{R}^{H \times W \times C}$  denotes an image with  $C$  colour channels, and  $\mathbf{y}^{in} \in \mathcal{Y}^{in} \subset \{0, 1\}^{H \times W \times Y}$  denotes the inlier pixel level labels that can belong to  $Y$  classes. We also have a set of outlier images and annotations  $\mathcal{D}^{out} = \{(\mathbf{x}_i, \mathbf{y}_i^{out})\}_{i=1}^{|\mathcal{D}^{out}|}$ , where  $\mathbf{y}^{out} \in \mathcal{Y}^{out} \subset \{0, 1\}^{H \times W \times (Y+1)}$  denotes the outlier pixel-level labels, with the class  $Y + 1$  reserved for pixels belonging to the anomaly class. Note that similarly to previous papers [5], the types of anomalies in training set  $\mathcal{D}^{out}$  do not overlap with the anomalies to be found in the testing set.

### 3.2. Pixel-wise Energy-biased Abstention Learning (PEBAL)

The PEBAL model is denoted by

$$p_\theta(y|\mathbf{x})_\omega = \frac{\exp(f_\theta(y; \mathbf{x})_\omega)}{\sum_{y' \in \{1, \dots, Y+1\}} \exp(f_\theta(y'; \mathbf{x})_\omega)}, \quad (1)$$

where  $\theta$  is the model parameter,  $\omega$  indexes a pixel in the image lattice  $\Omega$ ,  $p_\theta(y|\mathbf{x})_\omega$  represents the probability of labelling pixel  $\omega$  with  $y \in \{1, \dots, Y+1\}$ , and  $f_\theta(y; \mathbf{x})_\omega$  is the logit for class  $y$  at pixel  $\omega$ .

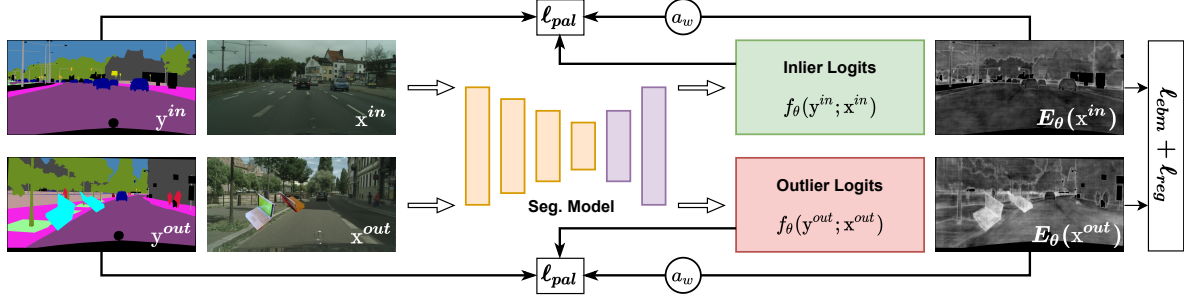


Figure 2. **PEBAAL**. The pixel-wise anomaly abstention (PAL) loss  $\ell_{pal}$  learns to abstain the prediction of outlier pixels from  $\mathbf{x}^{out}$  containing OE objects (i.e., cyan coloured masks) and calibrate the logit of inlier classes (i.e., reduction of the inlier logits) from both inlier image  $\mathbf{x}^{in}$  and outlier image  $\mathbf{x}^{out}$ . The EBM loss  $\ell_{ebm}$  pushes the free energy  $E_\theta$  to low values for inlier pixels and pulls that to high values for outlier pixels, where a regularisation loss  $\ell_{reg}$  enforces the smoothness and sparsity constraints on the energy maps. Such EBM learning reduces the logit of inlier classes to share similar values at the same time, facilitating the  $\ell_{pal}$  learning. Then, the pixel-wise penalty  $a_\omega$  associated with the abstention class at position  $\omega$  is estimated to bias the penalty to be low for outlier pixels and high for inlier pixels, which in turn encourages high free energy for anomalies and enforces  $\ell_{pal}$  to abstain the anomalous pixels.

To train the model in (1), we formulate a cost function that jointly trains PAL and EBM to classify anomalous pixels. An important training hyper-parameter for PAL is the penalty to abstain from the classification into one of the inlier classes in  $\{1, \dots, Y\}$ —this penalty is generally tuned to a single value for all training samples through model selection (e.g., cross validation) [31]. Instead of treating this as a tunable hyper-parameter, we propose the use of EBM (defined below in (4)) to automatically estimate this penalty during the training process for each pixel within each training image. More specifically, the cost function to train the PEBAAL model in (1) is:

$$\begin{aligned} \ell(\mathcal{D}^{in}, \mathcal{D}^{out}, \theta) = & \sum_{(\mathbf{x}, \mathbf{y}^{in}) \in \mathcal{D}^{in}} (\ell_{pal}(\theta, \mathbf{y}^{in}, \mathbf{x}, E_\theta(\mathbf{x})) + \lambda \ell_{ebm}^{in}(E_\theta(\mathbf{x})) + \ell_{reg}(E_\theta(\mathbf{x}))) + \\ & \sum_{(\mathbf{x}, \mathbf{y}^{out}) \in \mathcal{D}^{out}} (\ell_{pal}(\theta, \mathbf{y}^{out}, \mathbf{x}, E_\theta(\mathbf{x})) + \lambda \ell_{ebm}^{out}(E_\theta(\mathbf{x})) + \ell_{reg}(E_\theta(\mathbf{x}))). \end{aligned} \quad (2)$$

where  $\ell_{pal}(\cdot)$  denotes the PAL loss defined as

$$\ell_{pal}(\theta, \mathbf{y}, \mathbf{x}, E_\theta(\mathbf{x})) = -\sum_{\omega \in \Omega} \log \left( f_\theta(y_\omega; \mathbf{x})_\omega + \frac{f_\theta(Y+1; \mathbf{x})_\omega}{a_\omega} \right), \quad (3)$$

with  $y_\omega \in \{1, \dots, Y\}$  for  $\mathbf{y}^{in}$ ,  $y_\omega \in \{1, \dots, Y+1\}$  for  $\mathbf{y}^{out}$ , and  $a_\omega$  denotes the pixel-wise penalty associated with abstaining from the classification of the inlier classes. The minimisation of the loss in (3) will abstain from classifying outlier pixels into one of the inlier classes, where a pixel is estimated to be an outlier with  $a_\omega$ . Before formulating  $a_\omega$ , let us define the inlier free energy at pixel  $\omega$ , which is denoted by  $E_\theta(\mathbf{x})_\omega$  and computed with the *logsumexp* operator as follows [13, 23, 30]:

$$E_\theta(\mathbf{x})_\omega = -\log \sum_{y \in \{1, \dots, Y\}} \exp(f_\theta(y; \mathbf{x})_\omega). \quad (4)$$

The pixel-wise penalty associated with abstaining from the

classification of the inlier classes is defined by

$$a_\omega = (-E_\theta(\mathbf{x})_\omega)^2, \quad (5)$$

which means that the larger the  $a_\omega$  (i.e., low inlier free energy, so the sample is an inlier), the higher the loss to abstain from classifying into one of the  $Y$  classes, and low value of  $a_\omega$  (i.e., high free inlier energy, which means an outlier sample) implies a lower loss to abstain from classifying one of the  $Y$  classes. Also in (2),  $\ell_{ebm}^{in}(\cdot)$  (weighted by hyper-parameter  $\lambda$ ) represents the EBM loss that pushes the inlier free energy in (4) for samples in  $\mathcal{D}^{in}$  to low values, with

$$\ell_{ebm}^{in}(E_\theta(\mathbf{x})) = \sum_{\omega \in \Omega} (\max(0, E_\theta(\mathbf{x})_\omega - m_{in}))^2, \quad (6)$$

representing the loss of having inlier samples with free energy larger than threshold  $m_{in}$ , and

$$\ell_{ebm}^{out}(E_\theta(\mathbf{x})) = \sum_{\omega \in \Omega} (\max(0, m_{out} - E_\theta(\mathbf{x})_\omega))^2, \quad (7)$$

denoting the loss of having outlier samples with inlier free energy smaller than threshold  $m_{out}$ , where the margin losses in (6) and (7) effectively create an energy gap between normal and abnormal pixels. The last term to define in (2) is the inlier free energy regularisation loss to enforce that anomalous pixels are sparse and pixel anomaly classification is smooth (i.e., anomalous pixels tend to have anomalous neighbouring pixels), which is defined as

$$\ell_{reg}(E_\theta(\mathbf{x})) = \sum_{\omega \in \Omega} \beta_1 |E_\theta(\mathbf{x})_\omega - E_\theta(\mathbf{x})_{\mathcal{N}(\omega)}| + \beta_2 |E_\theta(\mathbf{x})_\omega|, \quad (8)$$

where  $\beta_1$  and  $\beta_2$  are hyper-parameters that weight the contributions of the smoothness and sparsity and sparsity regularisations, and  $\mathcal{N}(\omega)$  denotes neighbouring pixels in horizontal and vertical directions.



Different from maximising the uncertainty of anomalous pixels [19], our approach relies on PAL to explicitly learn the anomaly class  $Y + 1$  that fits all anomalous pixels from images in  $\mathcal{D}^{out}$ . The PAL optimisation in (3) is enforced to produce precise classification of inliers and outliers, but it lacks robustness due to i) the potential overfitting of the outliers from  $\mathcal{D}^{out}$  and ii) the sensitivity w.r.t. the penalty factor setting. On the other hand, the EBM optimisation in (6) and (7) can classify inliers and outliers robustly, so it can generalise to outliers outside  $\mathcal{D}^{out}$ , but it lacks precision because it provides a weak separation between the two classes. The joint training in PEBAL makes use of the robustness of EBM to regularise the anomaly class learning in PAL and enable the adaptive pixel-wise penalty estimation, while at the same time leveraging the classification precision of PAL, i.e., the learned inlier logits in  $\ell_{pal}$ , to boost the class separation capability in EBM and further improve its robustness. Hence, the joint optimisation of PAL and EBM in PEBAL is mutually beneficial towards learning a precise and robust pixel-wise anomaly classifier.

### 3.3. AnomalyMix, Training and Inference

An important point of the training process is how to setup the inlier and outlier datasets  $\mathcal{D}^{in}$  and  $\mathcal{D}^{out}$ . A recently published paper [5] carefully selects images to be included in  $\mathcal{D}^{out}$  by making sure that the segmentation labels presented in those images do not overlaps with the inlier labels. In particular for [5],  $\mathcal{D}^{in}$  has images and annotations from Cityscape and  $\mathcal{D}^{out}$  has images and annotations from COCO [28]. We argue that there are two issues with this strategy to form  $\mathcal{D}^{out}$ , which are: 1) the selected COCO images generally only contain anomalous pixel labels, leading to unstable training of the outlier losses (i.e., second summation in (2)) given the exclusive presence of the anomaly class (in effect, this becomes a one-class segmentation problem); 2) re-training the model with images containing only anomalous pixels removes the semantic context of inlier pixels when training for the outlier losses, which can deteriorate the segmentation accuracy of the inlier labels.

To mitigate these issues, we propose AnomalyMix, a method based on CutMix and CutPaste [26, 39] to form  $\mathcal{D}^{out}$ , where we cut the anomalous objects from an outlier dataset (e.g., COCO) using its labelled masks and paste them into the images of the inlier dataset (e.g., CitySpace), where we label the pixels of the anomalous object with the class  $Y + 1$  – these images are then inserted into  $\mathcal{D}^{out}$ . Our AnomalyMix addresses the two issues above because the outlier images now contain a combination of inlier and outlier pixels, allowing a balanced learning and keeping the visual context of inlier labels when training for the outlier losses. Furthermore, AnomalyMix can form a potentially infinite number of training images for  $\mathcal{D}^{out}$  given the range of transformations to be applied to the cut objects and the

locations of the inlier images that the objects can be pasted.

Previous papers [10, 19] argue that re-training the whole segmentation model can jeopardise the segmentation accuracy for the inlier classes. Furthermore, such re-training requires a long training time, leading to inefficient optimisation. In this work, we propose to **fine-tune only the final classification block** using the loss in (2), instead of re-training the whole segmentation model. Besides being efficient, this fast fine-tuning keeps the segmentation accuracy of the model in the original dataset used for pre-training the model. Furthermore, an interesting side-effect of our training is that the cost function in (2) will calibrate the segmentation prediction for the inlier classes. This happens because the terms  $\ell_{pal}(\cdot)$ ,  $\ell_{ebm}^{in}(\cdot)$  and  $\ell_{ebm}^{out}(\cdot)$  jointly constrain the maximisation of logits and naturally calibrate classification confidence.

During **inference**, pixel-wise anomaly detection is performed by computing the inlier free energy score  $\mathbb{E}_{\theta}(\mathbf{x})_{\omega}$  from (4) for each pixel position  $\omega$  given a test image  $\mathbf{x}$  and inlier segmentation is obtained from the inlier classes from the PEBAL model in (1). Following [19], we also apply a Gaussian smoothing kernel to produce the final energy map.

## 4. Experiment

### 4.1. Datasets

**LostAndFound** [35] is one of the first publicly available urban driving scene anomaly detection datasets containing real-world anomalous objects. The dataset has an official testing set containing 1,203 images with small obstacles in front of the cars, collecting from 13 different street scenes, featuring 37 different types of anomalous objects with various sizes and material.

**Fishyscapes** [4] is a high-resolution dataset for anomaly estimation in semantic segmentation for urban driving scenes. The benchmark has an online testing set that is entirely unknown to the methods. The dataset is composed by two data sources: Fishyscapes LostAndFound that contains a set of real road anomalous objects [35] and Fishyscapes Static that contains the blended anomalous objects from Pascal VOC [12]. For all datasets, we select the checkpoints based on the results on the public validation sets, but submitted our code and checkpoints to the benchmark website to be evaluated on their hidden test sets.

**Road Anomaly** [29] contains real-world road anomalies in front of the vehicles. The dataset has 60 images from the Internet, containing unexpected animals rocks, cones and obstacles. Unlike the LostAndFound and Fishyscapes, this dataset contains abnormal objects with various scales and sizes, making it even more challenging.

### 4.2. Implementation Details

Following [5, 10, 19], we use DeepLabv3+ [6] with WideResNet34 trained by Nvidia [40] and ResNet101

Table 1. Comparison with previous approaches on **Fishyscapes Leaderboard**. We achieve a new state-of-the-art performance among the approaches that require extra OoD data, and without re-training the segmentation networks and extra networks on Fishyscapes Leaderboard.

Models	re-training	Extra Network	OoD Data	FS LostAndFound		FS Static		mIoU $\uparrow$
				AP $\uparrow$	FPR95 $\downarrow$	AP $\uparrow$	FPR95 $\downarrow$	
Discriminative Outlier Detection Head [2]	✓	✓	✓	31.31	19.02	96.76	0.29	79.57
MSP [16]	✗	✗	✗	1.77	44.85	12.88	39.83	80.30
Entropy [17]	✗	✗	✗	2.93	44.83	15.41	39.75	80.30
SML [19]	✗	✗	✗	31.05	21.52	53.11	19.64	80.33
kNN Embedding - density [4]	✗	✗	✗	3.55	30.02	44.03	20.25	80.30
Bayesian Deeplab [33]	✓	✗	✗	9.81	38.46	48.70	15.05	73.80
Density - Single-layer NLL [4]	✗	✓	✗	3.01	32.9	40.86	21.29	80.30
Density - Minimum NLL [4]	✗	✓	✗	4.25	47.15	62.14	17.43	80.30
Image Resynthesis [29]	✗	✓	✗	5.70	48.05	29.6	27.13	81.40
OoD Training - Void Class	✓	✗	✓	10.29	22.11	45.00	19.40	70.40
Dirichlet Deeplab [32]	✓	✗	✓	34.28	47.43	31.30	84.60	70.50
Density - Logistic Regression [4]	✗	✓	✓	4.65	24.36	57.16	13.39	80.30
SynBoost [10]	✗	✓	✓	43.22	15.79	72.59	18.75	81.40
Ours	✗	✗	✓	<b>44.17</b>	<b>7.58</b>	<b>92.38</b>	<b>1.73</b>	90.53

Table 2. Anomaly segmentation results on **LostAndFound** testing set, with **WideResnet34** backbone. All methods use the same segmentation models. \* indicate that the model requires additional learnable parameters.  $\dagger$  indicates that the results are obtained from the official code with our WideResnet34 backbone.

Methods	AUC $\uparrow$	AP $\uparrow$	FPR <sub>95</sub> $\downarrow$	mIoU $\uparrow$
MSP [16]	85.49	38.20	18.56	90.72
Mahalanobis [25]	79.53	42.56	24.51	90.72
Max Logit [17]	94.52	65.45	15.56	90.72
Entropy [17]	86.52	50.66	16.95	90.72
Energy [30]	94.45	66.37	15.69	90.72
Meta-OoD [5]	97.95	71.23	5.95	89.74
$\dagger$ SML [19]	88.05	25.89	44.48	90.72
$\dagger$ SynBoost* [10]	97.53	7.71	69.12	90.72
Deep Gambler [31]	98.67	72.73	3.81	89.64
Ours	<b>99.76</b>	<b>78.29</b>	<b>0.81</b>	89.91

from [19] as the backbone of our segmentation models. The models are trained on Cityscapes [8] training set. For our PEBAL fine-tuning, we empirically set the  $m_{in}$  and  $m_{out}$  in Eq. 6 and Eq. 7 as -12 and -6, respectively. The weights  $\beta_1$  and  $\beta_2$  in Eq. 8 are set to  $5e - 4$  and  $3e - 6$ , and  $\lambda$  in Eq. 2 to 0.1. For LostAndFound testing set and Fishyscapes benchmarks, we set  $\lambda$  to 0.01 and 0.1 for the weight of  $\ell_{ebm}$ , respectively. Our training consists of fine-tuning the final classification block of the model for 20 epochs. We use the same resolution of random crop as in [40], and use Adam with a learning rate of  $1e^{-5}$  and  $1e^{-6}$  for Fishyscapes and LostAndFound testing sets, respectively. The batch size is set to 16. Following [5], for our AnomalyMix augmentation, we randomly sample 297 images as training data from the remaining COCO images that do not contain objects in Cityscapes or our anomaly validation/testing sets and randomly apply AnomalyMix to mix them into the Cityscape training images, following Chan et al. [5].

### 4.3. Evaluation Measures

Following [4, 5, 10, 19], we compute the the area under receiver operating characteristics (AUROC), average precision (AP), and the false positive rate at a true positive rate of 95% (FPR95) to validate our approach. For Fishyscapes public leaderboard, we use AP and FPR95 to compare with other methods, same as their website.

### 4.4. Comparison on LostAndFound

Table 2 shows the result on the testing set of LostAndFound. Notably, our approach surpasses the previous baseline approaches (i.e., MSP [16], Mahalanobis [25], Max Logit [17] and Entropy [17]) by 10% to 40% AP, and 14% to 23% FPR95, respectively. When compared with previous SOTA approaches such as SynBoost [10], SML [19] and Meta-OoD [5], we improve the AP performance by a large margin (15% to 40%), and decrease the FPR95 by about 5% to 70%. This illustrates the robustness and effectiveness on detecting small and distant anomalous objects given that the dataset contains mostly real-world small objects. Our PEBAL also improves the EBM baseline [30] and the AL baseline based on Deep Gambler [31]. This demonstrates that a simple adaptation of AL and EBM is not enough to enable accurate pixel-wise anomaly detection. It is worth noting that our approach achieves 0.81% FPR95, significantly reducing the false positive pixels, improving the chances of applying it to real-world applications. The marginal mIoU drop (of 0.8%) on Cityscapes is thus acceptable considering the large improvement on detecting anomalies.

### 4.5. Comparison on Fishyscapes and Road Anomaly

**Fishyscapes Leaderboard.** Table 1 shows the leaderboard results on the test set of Fishyscapes LostAndFound and Fishyscapes Static. Following [19], we compared the methods based on whether they require re-training of the entire segmentation network, adding the extra network, or

Table 3. Anomaly segmentation results on **Fishyscapes validation sets** (LostAndFound and Static), and the **Road Anomaly testing set**, with **WideResnet34** backbone. \* indicate that the model requires additional learnable parameters. † indicates that the results are obtained from the official code with our WideResnet34 backbone.

Methods	FS LostAndFound			FS Static			Road Anomaly			mIoU ↑
	AUC ↑	AP ↑	FPR <sub>95</sub> ↓	AUC ↑	AP ↑	FPR <sub>95</sub> ↓	AUC ↑	AP ↑	FPR <sub>95</sub> ↓	
MSP [16]	89.29	4.59	40.59	92.36	19.09	23.99	67.53	15.72	71.38	90.72
Max Logit [16]	93.41	14.59	42.21	95.66	38.64	18.26	72.78	18.98	70.48	90.72
Entropy [17]	90.82	10.36	40.34	93.14	26.77	23.31	68.80	16.97	71.10	90.72
Energy [30]	93.72	16.05	41.78	95.90	41.68	17.78	73.35	19.54	70.17	90.72
Mahalanobis [25]	96.75	56.57	11.24	96.76	27.37	11.7	62.85	14.37	81.09	90.72
Meta-OoD [10]	93.06	41.31	37.69	97.56	72.91	13.57	-	-	-	89.78
†Synboost* [10]	96.21	60.58	31.02	95.87	66.44	25.59	81.91	38.21	64.75	90.72
†SML [19]	94.97	22.74	33.49	97.25	66.72	12.14	75.16	17.52	70.70	90.72
Deep Gambler [31]	97.82	31.34	10.16	98.88	84.57	3.39	78.29	23.26	65.12	90.19
Ours	<b>98.96</b>	<b>58.81</b>	<b>4.76</b>	<b>99.61</b>	<b>92.08</b>	<b>1.52</b>	<b>87.63</b>	<b>45.10</b>	<b>44.58</b>	90.53

Table 4. Ablation studies for anomaly segmentation on **LostAndFound**, with **WideResnet34** backbone. CE+COCO denotes the cross entropy loss trained with an extra OoD class (i.e., COCO images), AL denotes the baseline abstention learning [31], and AM represents the AnomalyMix augmentation.

CE+COCO	AM	AL	$\ell_{ebm}$	$\ell_{pal}$	$\ell_{reg}$	AUC ↑	AP ↑	FPR <sub>95</sub> ↓
✓						95.37	65.54	13.69
✓	✓					96.88	69.02	8.03
	✓	✓				98.67	72.73	3.81
	✓	✓	✓			99.04	73.21	2.97
	✓		✓	✓		99.63	77.19	1.19
	✓		✓	✓	✓	<b>99.76</b>	<b>78.29</b>	<b>0.81</b>

utilising the OoD data. We achieve the SOTA performance by a large margin on Fishyscapes leaderboard when compared with the previous methods except [2] (Static) that rely on an inefficient re-training segmentation model, a large extra network, extra OoD training data and ensemble anomaly scores. Without re-training the entire network or adding extra learnable parameters, our approach can work efficiently to surpass previous SOTA competing approaches that fall into the same category by about 13% to 42% on LostAndFound and 40% to 50% AP on Static. Moreover, it is worth noting that PEBAL reduces the amount of false positive pixels to 7.58 and 1.73 FPR on the two datasets. This result is publicly available on the Fishyscapes website.

**Fishyscapes validation sets and Road Anomaly.** In Tables 3 and 5, we compare our approach on the Fishyscapes validation sets and Road Anomaly using two different backbones. Our model outperforms the previous methods by a large margin on all three benchmarks, regardless of the backbones and their segmentation accuracy. To verify the applicability of our method, except for the modern WideResnet34 backbone (90.7 mIoU on Cityscapes), we use a ResNet101 DeepLabv3+ (80.3 mIoU on Cityscapes) to investigate the performance in terms of the size of the architecture and its inlier segmentation accuracy. The results demonstrate that our approach is applicable to a wide-range

of segmentation models, indicating the effectiveness of PEBAL to adapt to real-world systems. Moreover, our fine-tuning sacrifices only marginally the inlier segmentation accuracy for both backbones, achieving good performance on both inlier and anomaly segmentation.

#### 4.6. Ablation Study

Table 4 shows the contribution of each component of our PEBAL on the LostAndFound testing set. Our PEBAL obtains a significant performance gain by adding the AnomalyMix to the cross-entropy baseline that is directly trained to classify the anomalous pixels. Previous image-level AL improves the performance to 72.73% and 3.81% AP and FPR, respectively. A simple combination of  $\ell_{ebm}$  and AL only improves the performance to 73.21% AP and 2.97% FPR. When adapting the proposed adaptive energy-biased penalty  $a_\omega$  and  $\ell_{ebm}$  to consider the pixel-wise information, the performance is boosted to 77.19% AP and 1.19% FPR95. Finally, the smoothness and sparsity regularisation losses stabilise the training and further improve the performance to the best results.

#### 4.7. Outlier Samples, Calibration and Efficiency

**Outlier Diversity and Efficiency.** In Table 6, we randomly select 1%, 5%, 10%, 25% 50%, and 75% of COCO classes as the OE data during training and compute the mean results over three different random seeds. We achieve consistent AP and FPR performance regardless of the number of COCO classes used during the training on Fishyscapes. It is also worth noting that our approach can effectively learn the PEBAL model using **only one class** (1% in Table 6) of outlier data, which selects some of the irrelevant classes of COCO objects that are not possible to be found on road in real life (e.g., dining table, laptop, and clock). The results indicate that our model can consistently achieve SOTA performance on Fishyscapes without a careful selection of OE classes, demonstrating the robustness of our approach under diverse outlier classes. We also

Table 5. Anomaly segmentation results on **Fishyscapes validation sets** (LostAndFound and Static), and the **Road Anomaly testing set**, with **Resnet101** backbone. \* indicate that the model requires additional learnable parameters. † indicates that the results are obtained from the official code with our Resnet101 backbone.

Methods	FS LostAndFound			FS Static			Road Anomaly			mIoU ↑
	AUC ↑	AP ↑	FPR <sub>95</sub> ↓	AUC ↑	AP ↑	FPR <sub>95</sub> ↓	AUC ↑	AP ↑	FPR <sub>95</sub> ↓	
MSP [16]	86.99	6.02	45.63	88.94	14.24	34.10	73.76	20.59	68.44	80.33
Max Logit [16]	92.00	18.77	38.13	92.80	27.99	28.50	77.97	24.44	64.85	80.33
Entropy [17]	88.32	13.91	44.85	89.99	21.78	33.74	75.12	22.38	68.15	80.33
Energy [30]	93.50	25.79	32.26	91.28	31.66	37.32	78.13	24.44	63.36	80.33
†SynthCP* [38]	88.34	6.54	45.95	89.9	23.22	34.02	76.08	24.86	64.69	80.33
†Synboost* [10]	94.89	40.99	34.47	92.03	48.44	47.71	85.23	41.83	59.72	80.33
SML [19]	96.88	36.55	14.53	96.69	48.67	16.75	81.96	25.82	49.74	80.33
Deep Gambler [31]	97.19	39.77	12.41	97.51	67.69	15.39	85.45	31.45	48.79	78.97
Ours	<b>99.09</b>	<b>59.83</b>	<b>6.49</b>	<b>99.23</b>	<b>82.73</b>	<b>6.81</b>	<b>92.51</b>	<b>62.37</b>	<b>28.29</b>	79.58

Table 6. The performance comparison of our approach on Fishyscapes benchmark w.r.t different **diversity of OE classes** (mean results over three random seeds), in terms of AP and FPR95.

Class Per.	FS LostAndFound		FS Static	
	AP ↑	FPR <sub>95</sub> ↓	AP ↑	FPR <sub>95</sub> ↓
1%	57.23 ±2.37	6.49 ±1.98	86.14 ±1.26	2.84 ±0.89
5%	50.84 ±3.41	7.69 ±2.94	89.61 ±1.98	2.29 ±0.69
10%	54.98 ±2.79	5.95 ±1.36	91.21 ±1.14	1.59 ±0.47
25%	53.58 ±4.35	6.84 ±1.08	90.01 ±0.87	1.68 ±0.11
50%	56.58 ±2.37	5.54 ±1.27	91.72 ±0.69	1.65 ±0.08
75%	57.67 ±3.35	5.18 ±1.79	91.24 ±0.81	1.73 ±0.13

Table 7. The performance comparison of our approach on Fishyscapes benchmark w.r.t different **amount of OE training samples** (mean results over three random seeds), in terms of AP and FPR95.

Train Size	FS LostAndFound		FS Static	
	AP ↑	FPR <sub>95</sub> ↓	AP ↑	FPR <sub>95</sub> ↓
5%	54.63 ±2.06	5.19 ±2.03	89.42 ±1.57	2.07 ±0.96
10%	56.28 ±0.96	4.97 ±1.19	89.95 ±0.89	1.78 ±0.18
25%	55.63 ±1.78	5.01 ±1.23	90.74 ±0.78	1.79 ±0.26
50%	57.03 ±1.43	4.84 ±1.49	91.67 ±1.79	1.68 ±0.84

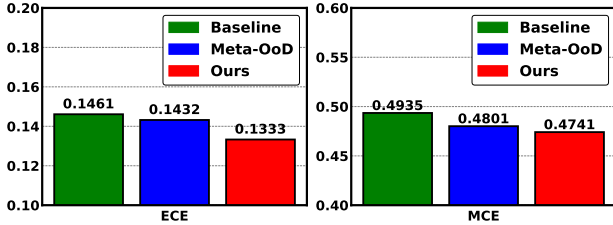


Figure 3. Confidence calibration performances between WideResnet34 baseline, Meta-OoD [5], and our approach.

investigate the outlier sample efficiency of our model w.r.t smaller OE training sets with a fixed 100% COCO classes (80 classes) on Fishyscapes in Table 7, and we achieve consistently good performance regardless the number of outlier training samples. All those experiments show the applicability of our PEBAL to real-world autonomous driving systems.

**Confidence Calibration.** In Fig. 3, we show that our model can also improve the calibration of the segmentation confidence. This figure shows that we improve the ECE and MCE [14] scores by a small margin, showing another benefit of using our PEBAL approach.

**Computational Efficiency.** We compare the efficiency of the training of PEBAL with Meta-OoD [5] in terms of the trainable parameters and training time. As PEBAL requires the fine-tuning of the final classification block, it has only 1.3 M parameters with about 12 min. training time

per epoch, which is significantly less than the re-training approach (Meta-OoD) that needs 137.1 M parameters with around 26 min. training time per epoch.

## 5. Conclusions and Discussions

We proposed a simple yet effective approach, named Pixel-wise Energy-biased Abstention Learning (PEBAL), to fine-tune the last block of a segmentation model to detect unexpected road anomalies. The approach introduces a non-trivial training that jointly optimises a novel pixel-wise abstention learning and an energy-based model to learn an adaptive pixel-wise anomaly class, in which a new pixel-wise energy-biased penalty estimation method is proposed to improve the precision and robustness to detect small and distant anomalous objects. The resulting model significantly reduces the false positive and false negative detected anomalies, compared with previous SOTA methods. The results on four benchmarks demonstrate the accuracy and robustness of our approach to detect anomalous objects regardless of the amount or diversity of exposed training outliers. Despite the remarkable performance on most datasets, PEBAL is not as effective on the most challenging dataset, Road Anomaly, that contains significantly more diverse and realistic anomalous objects. We plan to further enhance the generalisation of our model to accurately detect more unknown, diverse anomalies.



## References

- [1] Christoph Baur, Benedikt Wiestler, Shadi Albarqouni, and Nassir Navab. Deep autoencoding models for unsupervised anomaly segmentation in brain mr images. In *International MICCAI Brainlesion Workshop*, pages 161–169. Springer, 2018. [3](#)
- [2] Petra Bevandi et al. Simultaneous semantic segmentation and outlier detection in presence of domain shift. In *German Conference on Pattern Recognition*, pages 33–47. Springer, 2019. [2](#), [3](#), [6](#), [7](#)
- [3] Petra Bevandić, Ivan Krešo, Marin Oršić, and Siniša Šegvić. Discriminative out-of-distribution detection for semantic segmentation. *arXiv preprint arXiv:1808.07703*, 2018. [3](#)
- [4] Hermann Blum, Paul-Edouard Sarlin, Juan Nieto, Roland Siegwart, and Cesar Cadena. The fishyscapes benchmark: Measuring blind spots in semantic segmentation. *arXiv preprint arXiv:1904.03215*, 2019. [2](#), [3](#), [5](#), [6](#)
- [5] Robin Chan, Matthias Rottmann, and Hanno Gottschalk. Entropy maximization and meta classification for out-of-distribution detection in semantic segmentation. In *Proceedings of the IEEE/CVF International Conference on Computer Vision*, pages 5128–5137, 2021. [1](#), [2](#), [3](#), [5](#), [6](#), [8](#)
- [6] Liang-Chieh Chen, Yukun Zhu, George Papandreou, Florian Schroff, and Hartwig Adam. Encoder-decoder with atrous separable convolution for semantic image segmentation. In *Proceedings of the European conference on computer vision (ECCV)*, pages 801–818, 2018. [5](#)
- [7] Yuanhong Chen, Yu Tian, Guansong Pang, and Gustavo Carneiro. Deep one-class classification via interpolated gaussian descriptor. 2021. [3](#)
- [8] Marius Cordts, Mohamed Omran, Sebastian Ramos, Timo Rehfeld, Markus Enzweiler, Rodrigo Benenson, Uwe Franke, Stefan Roth, and Bernt Schiele. The cityscapes dataset for semantic urban scene understanding. In *Proceedings of the IEEE conference on computer vision and pattern recognition*, pages 3213–3223, 2016. [3](#), [6](#)
- [9] Clement Creusot and Asim Munawar. Real-time small obstacle detection on highways using compressive rbm road reconstruction. In *2015 IEEE Intelligent Vehicles Symposium (IV)*, pages 162–167. IEEE, 2015. [3](#)
- [10] Giancarlo Di Biase, Hermann Blum, Roland Siegwart, and Cesar Cadena. Pixel-wise anomaly detection in complex driving scenes. In *Proceedings of the IEEE/CVF Conference on Computer Vision and Pattern Recognition*, pages 16918–16927, 2021. [2](#), [3](#), [5](#), [6](#), [7](#), [8](#)
- [11] Ran El-Yaniv et al. On the foundations of noise-free selective classification. *Journal of Machine Learning Research*, 11(5), 2010. [3](#)
- [12] Mark Everingham, Luc Van Gool, Christopher KI Williams, John Winn, and Andrew Zisserman. The pascal visual object classes (voc) challenge. *International journal of computer vision*, 88(2):303–338, 2010. [5](#)
- [13] Will Grathwohl, Kuan-Chieh Wang, Jörn-Henrik Jacobsen, David Duvenaud, Mohammad Norouzi, and Kevin Swersky. Your classifier is secretly an energy based model and you should treat it like one. *arXiv preprint arXiv:1912.03263*, 2019. [2](#), [3](#), [4](#)
- [14] Chuan Guo, Geoff Pleiss, Yu Sun, and Kilian Q Weinberger. On calibration of modern neural networks. In *International Conference on Machine Learning*, pages 1321–1330. PMLR, 2017. [8](#)
- [15] David Haldimann, Hermann Blum, Roland Siegwart, and Cesar Cadena. This is not what i imagined: Error detection for semantic segmentation through visual dissimilarity. *arXiv preprint arXiv:1909.00676*, 2019. [3](#)
- [16] Dan Hendrycks, Steven Basart, Mantas Mazeika, Mohammadreza Mostajabi, Jacob Steinhardt, and Dawn Song. Scaling out-of-distribution detection for real-world settings. *arXiv preprint arXiv:1911.11132*, 2019. [3](#), [6](#), [7](#), [8](#)
- [17] Dan Hendrycks and Kevin Gimpel. A baseline for detecting misclassified and out-of-distribution examples in neural networks. *arXiv preprint arXiv:1610.02136*, 2016. [3](#), [6](#), [7](#), [8](#)
- [18] Dan Hendrycks, Mantas Mazeika, and Thomas Dietterich. Deep anomaly detection with outlier exposure. *arXiv preprint arXiv:1812.04606*, 2018. [2](#), [3](#)
- [19] Sanghun Jung, Jungsoo Lee, Daehoon Gwak, Sungha Choi, and Jaegul Choo. Standardized max logits: A simple yet effective approach for identifying unexpected road obstacles in urban-scene segmentation. In *Proceedings of the IEEE/CVF International Conference on Computer Vision*, pages 15425–15434, 2021. [2](#), [3](#), [5](#), [6](#), [7](#), [8](#)
- [20] Alex Kendall and Yarin Gal. What uncertainties do we need in bayesian deep learning for computer vision? *arXiv preprint arXiv:1703.04977*, 2017. [3](#)
- [21] Balaji Lakshminarayanan, Alexander Pritzel, and Charles Blundell. Simple and scalable predictive uncertainty estimation using deep ensembles. *arXiv preprint arXiv:1612.01474*, 2016. [3](#)
- [22] Fahad Lateef and Yassine Ruichek. Survey on semantic segmentation using deep learning techniques. *Neurocomputing*, 338:321–348, 2019. [2](#)
- [23] Yann LeCun, Sumit Chopra, Raia Hadsell, M Ranzato, and F Huang. A tutorial on energy-based learning. *Predicting structured data*, 1(0), 2006. [2](#), [3](#), [4](#)
- [24] Kimin Lee, Honglak Lee, Kibok Lee, and Jinwoo Shin. Training confidence-calibrated classifiers for detecting out-of-distribution samples. *arXiv preprint arXiv:1711.09325*, 2017. [3](#)
- [25] Kimin Lee, Kibok Lee, Honglak Lee, and Jinwoo Shin. A simple unified framework for detecting out-of-distribution samples and adversarial attacks. *Advances in neural information processing systems*, 31, 2018. [6](#), [7](#)
- [26] Chun-Liang Li, Kihyuk Sohn, Jinsung Yoon, and Tomas Pfister. Cutpaste: Self-supervised learning for anomaly detection and localization. In *Proceedings of the IEEE/CVF Conference on Computer Vision and Pattern Recognition*, pages 9664–9674, 2021. [5](#)
- [27] Shiyu Liang, Yixuan Li, and Rayadurgam Srikant. Enhancing the reliability of out-of-distribution image detection in neural networks. *arXiv preprint arXiv:1706.02690*, 2017. [3](#)
- [28] Tsung-Yi Lin, Michael Maire, Serge Belongie, James Hays, Pietro Perona, Deva Ramanan, Piotr Dollár, and C Lawrence Zitnick. Microsoft coco: Common objects in context. In *European conference on computer vision*, pages 740–755. Springer, 2014. [5](#)

- [29] Krzysztof Lis, Krishna Nakka, Pascal Fua, and Mathieu Salzmann. Detecting the unexpected via image resynthesis. In *Proceedings of the IEEE/CVF International Conference on Computer Vision*, pages 2152–2161, 2019. 2, 3, 5, 6
- [30] Weitang Liu, Xiaoyun Wang, John D Owens, and Yixuan Li. Energy-based out-of-distribution detection. *arXiv preprint arXiv:2010.03759*, 2020. 2, 3, 4, 6, 7, 8
- [31] Ziyin Liu, Zhikang Wang, Paul Pu Liang, Russ R Salakhutdinov, Louis-Philippe Morency, and Masahito Ueda. Deep gamblers: Learning to abstain with portfolio theory. *Advances in Neural Information Processing Systems*, 32:10623–10633, 2019. 2, 4, 6, 7, 8
- [32] Andrey Malinin and Mark Gales. Predictive uncertainty estimation via prior networks. *arXiv preprint arXiv:1802.10501*, 2018. 6
- [33] Jishnu Mukhoti and Yarin Gal. Evaluating bayesian deep learning methods for semantic segmentation. *arXiv preprint arXiv:1811.12709*, 2018. 2, 3, 6
- [34] Erik Nijkamp, Mitch Hill, Song-Chun Zhu, and Ying Nian Wu. Learning non-convergent non-persistent short-run mcmc toward energy-based model. *arXiv preprint arXiv:1904.09770*, 2019. 3
- [35] Peter Pinggera, Sebastian Ramos, Stefan Gehrig, Uwe Franke, Carsten Rother, and Rudolf Mester. Lost and found: detecting small road hazards for self-driving vehicles. In *2016 IEEE/RSJ International Conference on Intelligent Robots and Systems (IROS)*, pages 1099–1106. IEEE, 2016. 2, 5
- [36] Yu Tian, Guansong Pang, Yuanhong Chen, Rajvinder Singh, Johan W Verjans, and Gustavo Carneiro. Weakly-supervised video anomaly detection with robust temporal feature magnitude learning. *arXiv preprint arXiv:2101.10030*, 2021. 2
- [37] Simon Vandenhende, Stamatios Georgoulis, Marc Proesmans, Dengxin Dai, and Luc Van Gool. Revisiting multi-task learning in the deep learning era. *arXiv preprint arXiv:2004.13379*, 2, 2020. 3
- [38] Yingda Xia, Yi Zhang, Fengze Liu, Wei Shen, and Alan L Yuille. Synthesize then compare: Detecting failures and anomalies for semantic segmentation. In *European Conference on Computer Vision*, pages 145–161. Springer, 2020. 2, 3, 8
- [39] Sangdoo Yun, Dongyoon Han, Seong Joon Oh, Sanghyuk Chun, Junsuk Choe, and Youngjoon Yoo. Cutmix: Regularization strategy to train strong classifiers with localizable features. In *Proceedings of the IEEE/CVF International Conference on Computer Vision*, pages 6023–6032, 2019. 5
- [40] Yi Zhu, Karan Sapra, Fitsum A Reda, Kevin J Shih, Shawn Newsam, Andrew Tao, and Bryan Catanzaro. Improving semantic segmentation via video propagation and label relaxation. In *Proceedings of the IEEE/CVF Conference on Computer Vision and Pattern Recognition*, pages 8856–8865, 2019. 5, 6